Published in final edited form as:
Nat Methods. 2009 December ; 6(12): 905. doi:10.1038/nmeth.1400.

Cell stimulation with optically manipulated microsources

Holger Kress[1], **Jin-Gyu Park**[1], **Cecile O Mejean**[1], **Jason D Forster**[1], **Jason Park**[2], **Spencer S Walse**[3,8], **Yong Zhang**[4], **Dianqing Wu**[4], **Orion D Weiner**[5], **Tarek M Fahmy**[2,3], and **Eric R Dufresne**[1,3,6,7]

[1]Department of Mechanical Engineering, Yale University, New Haven, Connecticut, USA.

[2]Department of Biomedical Engineering, Yale University, New Haven, Connecticut, USA.

[3]Department of Chemical Engineering, Yale University, New Haven, Connecticut, USA.

[4]Vascular Biology and Therapeutics Program and Department of Pharmacology, Yale University School of Medicine, New Haven, Connecticut, USA.

[5]Department of Biochemistry, University of California, San Francisco, San Francisco, California, USA.

[6]Department of Physics, Yale University, New Haven, Connecticut, USA.

[7]Department of Cell Biology, Yale University, New Haven, Connecticut, USA.

Abstract

Molecular gradients are important for various biological processes including the polarization of tissues and cells during embryogenesis and chemotaxis. Investigations of these phenomena require control over the chemical microenvironment of cells. We present a technique to set up molecular concentration patterns that are chemically, spatially and temporally flexible. Our strategy uses optically manipulated microsources, which steadily release molecules. Our technique enables the control of molecular concentrations over length scales down to about 1 μm and timescales from fractions of a second to an hour. We demonstrate this technique by manipulating the motility of single human neutrophils. We induced directed cell polarization and migration with microsources loaded with the chemoattractant formyl-methionine-leucine-phenylalanine. Furthermore, we triggered highly localized retraction of lamellipodia and redirection of polarization and migration with microsources releasing cytochalasin D, an inhibitor of actin polymerization.

Gradients of molecules are important for cell differentiation during embryonic development[1,2], for food gathering of single cellular organisms[3–5] and for the immune response of higher organisms[6]. Chemotaxis, the directed migration of a cell along a chemical gradient, is a key element of the mammalian immune system[4,5,7,8]. Prokaryotes and eukaryotes have different mechanisms of chemotaxis: whereas bacteria temporally sense gradients and exhibit a biased random walk[3], eukaryotes can spatially sense gradients and regulate the actin

Correspondence should be addressed to H.K.(holger.kress@yale.edu) or E.R.D. (eric.dufresne@yale.edu).
[8]Present address: US Department of Agriculture, Parlier, California, USA.

Note: Supplementary information is available on the Nature Methods website.

AUTHOR CONTRIBUTIONS

H.K. and E.R.D. designed and performed the research, analyzed data and wrote the paper. J.G.P., J.D.F., S.S.W. and O.D.W. performed research and analyzed data. C.O.M. and Y.Z. performed research. J.P. and T.M.F. designed research and contributed new reagents and analytic tools. D.W. designed research.

cytoskeleton to migrate toward sources of chemoattractant[4,5,7,8]. Over the past decade, mathematical models of eukaryotic chemotaxis have matured and incorporated various biochemical reaction-diffusion schemes[9,10]. Different models describe qualitatively different modes of gradient sensing and show qualitatively different spatial and temporal dynamics. To test predictions from competing models in experiments, precise control over chemical microenvironments of cells is needed.

Established techniques to create linear or radial gradients of soluble molecules have used diffusion chambers and micropipettes. Emerging techniques that incorporate microfluidic devices[11,12], photoinduced uncaging[12,13] or photolysis of nanoparticles[14] allow more control over the geometry and the dynamics of the molecular concentration patterns. However, there is so far no technique available that allows the creation of persistent gradient patterns that can be flexibly shaped in three dimensions down to micrometer scales.

Here we present a strategy for cell stimulation that enables the control of concentrations of soluble molecules over length scales from about 100 μm to 1 μm at timescales from hours to a fraction of a second. This strategy is based on optically manipulated microsources (OMMs), microparticles that provide a controlled release of soluble molecules that act as chemoattractants or perturb the actin cytoskeleton. We individually trapped multiple microsources and independently manipulated them with holographic optical tweezers[15–17].

RESULTS

Microsource fabrication and structure

We fabricated microsources releasing the chemoattractant formyl-methionine-leucine-phenylalanine (fMLP; 438 g mol^{-1}) and microsources releasing the actin polymerization inhibitor cytochalasin D (508 g mol^{-1})[18,19] from polylactic-co-glycolic acid (PLGA) using a solvent evaporation–spontaneous emulsion technique[20]. Particles releasing fMLP stimulated chemotactic responses in single neutrophil-differentiated HL-60 cells, and particles releasing cytochalasin D perturbed the actin cytoskeleton of single HL-60 cells with high spatial localization.

The nominal loading (mass of the loaded chemical divided by the total mass of the loaded chemical and PLGA) was 0.01–0.17. We measured the structure of the PLGA particles by scanning electron microscopy (SEM). The SEM image (Supplementary Fig. 1) revealed that the particles were spherical. We measured the size distribution of the beads by SEM and by dynamic light scattering. The particles had a mean diameter of 500–1,000 nm and an average polydispersity (s.d. of diameter divided by mean diameter) of ~40%.

Controlled release of encapsulated agents

We determined the concentration profile of molecules released from a microsource close to a coverslip by the release rate, the diffusion coefficient of the released molecule and the boundary condition imposed by the impenetrable coverslip. The concentration profile around a particle at a height h above a coverslip was approximated (derivation in Supplementary Note 1) by

$$c(\rho,z)=c_b+c_0\times a\left(\frac{1}{\left(\rho^2+(z+h)^2\right)^{\frac{1}{2}}}+\frac{1}{\left(\rho^2+(z-h)^2\right)^{\frac{1}{2}}}\right) \quad (1)$$

in which a is the particle radius, ρ and z are the cylindrical coordinates, c_0 is the concentration on the surface of the bead and c_b is the homogeneous background concentration. The concentration on the surface of the bead,

$$c_0 = j_0 \times \frac{a}{D} \tag{2}$$

was determined by the flux, j_0, of molecules from the particle surface and the diffusion coefficient, D, of the molecules. This equation is only exact when $h \gg a$. An example for a concentration profile around a particle is shown in Supplementary Figure 2.

To estimate the flux from individual beads, we measured the release of fMLP from ensembles of PLGA beads (Supplementary Note 1). Beads at a concentration of 1 mg ml^{-1} released 60 μM of fMLP during the first hour after suspending the beads in buffer solution. Release measurements on individual PLGA particles loaded with the fluorescent dye rhodamine B showed that the release rate was proportional to the bead volume (Supplementary Note 2 and Supplementary Fig. 3). Assuming the same particle size–dependence for fMLP yielded a flux of j_0 = 5,000 molecules μm^{-2} s^{-1} (60,000 molecules per second) from a microsource with a diameter of 2 μm. Using equation 2 and the diffusion coefficient of fMLP, D = ~1,000 μm^2 s^{-1}, the estimated concentration on the surface of the bead was therefore c_0 = 8 nM.

The concentration distribution of fMLP around a single microsource was sufficient to induce chemotaxis. If a 2-μm bead were placed near the membrane of a cell with a diameter of 20 μm, the cell would be exposed to an fMLP concentration of about 8 nM at the side facing the bead and a concentration of 0.2 nM at the opposite side if no homogeneous background concentration was present. If the background concentration is the dissociation constant (K_d) (~10 nM) for fMLP binding to its receptor[11], the front of the cell is exposed to an 80% larger concentration than the back of the cell. Concentration differences on that order of magnitude at an ambient concentration with a value of approximately the K_d value can induce chemotaxis in neutrophils[11].

Cell response to microsources of chemoattractants

Differentiated HL-60 cells are a neutrophil-like cell line that is used as a model system for studying neutrophil chemotaxis[21]. In positive control experiments, we characterized the migration of HL-60 cells in gradients of fMLP in a Zigmond diffusion chamber[22]. The potency of fMLP to stimulate chemotaxis was not reduced when it was encapsulated and released from PLGA beads (Supplementary Note 3 and Supplementary Fig. 4). By using HL-60 cells transfected with *YFP-actin* plasmid, we found that freely diffusing fMLP-loaded PLGA beads induced cell polarization and actin accumulation (Supplementary Fig. 5).

Individual optically trapped PLGA microparticles loaded with fMLP could induce a chemotactic response in single neutrophils. We introduced the microparticles to samples of HL-60 cells plated on coverslips and imaged the cells by differential interference contrast microscopy. We assayed the interaction of a cell with a single fMLP-loaded particle manipulated with holographic optical tweezers (Fig. 1 and Supplementary Video 1). We moved an individual fMLP-loaded particle close to the membrane of a neutrophil (Fig. 1a). The cell started to polarize and migrate in the direction of the particle (Fig. 1b). We then moved the particle counter-clockwise around the cell, and the cell changed its polarization and migration directions in response to the altered particle position (Fig. 1c–f). We estimated fMLP concentration around the bead (Fig. 1). The influence of the motion of the bead on the concentration pattern was negligible. In this and subsequent cell stimulation experiments, we moved the particles at speeds not exceeding 1 μm s^{-1}. At such low speeds, the steady-state

solution (equation 1) was a good approximation for the concentration distribution at any time (Supplementary Note 4). Furthermore, the presence of a cell changed the concentration pattern around a bead only negligibly (Supplementary Note 5 and Supplementary Fig. 6).

We analyzed the time-dependent orientation and motion of the cell (Fig. 1g,h) to determine whether it followed the bead motion: we extracted the cell position, the direction of the cell orientation and the direction of the gradient of fMLP from each of the time-lapse images. The angle that quantified the direction of the gradient increased continuously with time (Fig. 1i). The cell orientation could not be defined at the earliest time points (time $t \leq 25$ s) because the cell was lacking a leading edge. After the cell created a leading edge, the cell orientation followed the gradient direction with a time delay of up to 60 s. The cell responded to the stimulus created by the bead by polarizing and migrating in the direction of the stimulus. Upon first exposure to the bead, the cell reached a peak velocity of more than 15 μm min^{-1}, which decreased to ~7–13 μm min^{-1} for the remainder of the experiment (Fig. 1j). An additional movie of a single HL-60 cell stimulation with an individual optically trapped PLGA particle loaded with fMLP is shown in Supplementary Video 2.

The capability to trap and manipulate multiple microsources simultaneously offers a high degree of spatial flexibility for the creation of cell stimulus patterns that are not easily achieved with micropipettes. We assayed the response of a single HL-60 cell to a highly localized bipolar stimulus created with two optically trapped beads releasing fMLP (Fig. 2 and Supplementary Video 3). Upon positioning of the beads close to the cell, the cell formed a lamellipodium, which broadened as it advanced toward the well-separated beads.

Control experiments with optically manipulated unloaded PLGA beads showed no chemotactic response of the cells (Supplementary Videos 4 and 5). Furthermore, we quantified the heating of the trapped particles owing to the laser tweezers by using the temperature-dependent fluorescent dye Rhodamine B. The intensity of the fluorescence emitted from Rhodamine B decreases by 2.3% per 1 °C temperature increase[23]. For the trapping powers used in this study (~5 mW) the particles heated up by less than 0.1 °C (Supplementary Note 6 and Supplementary Fig. 7). As the plain PLGA beads did not affect the cell behavior, this temperature increase is negligible.

Cell response to actin polymerization inhibitors

We manipulated the motility of neutrophils using beads releasing the actin polymerization inhibitor cytochalasin D in the presence of a homogeneous background concentration of 100 nM fMLP. OMMs created highly localized stimuli, which induced strongly localized cytoskeletal perturbations (Fig. 3 and Supplementary Video 6). We stimulated an HL-60 cell with two optically trapped beads releasing cytochalasin D. We positioned the beads close to each other and to the center of the lamellipodium. After about 45 s, the lamellipodium started to retract at 10 μm min^{-1} in a small region around the beads. As a result, the lamellipodium was initially split into two parts. About 1 minute after the split, one of the two lamellipodia retracted while the other one persisted.

Bipolar perturbations caused notable changes to cell motility. We positioned two beads, separated by ~20 μm, in front of a migrating cell (Fig. 4 and Supplementary Video 7). The cell squeezed through the narrow gap created by the two microsources: the lamellipodium retracted on the two sides closest to the beads while the central part of the lamellipodium continued to progress. To analyze the response of an HL-60 cell to a temporally varying bipolar perturbation with cytochalasin D, we first stopped cell migration with two microsources (Fig. 5a,b and Supplementary Video 8). Then, we repositioned the two beads on two opposing ends of the cell along the direction of cell polarization. Subsequently, the cell repolarized in a direction perpendicular to the axis defined by the beads (Fig. 5c–f).

Holographic optical tweezers provide a high degree of spatial flexibility for the creation of molecular concentration patterns through their ability to independently manipulate multiple particles. We assayed this flexibility by stimulating single cells simultaneous with three or five microsources (Supplementary Fig. 8). Furthermore, the dynamic reconfiguration of optical traps provided a high degree of temporal flexibility. Our holographic optical tweezers[17] setup allowed us to move individual microsources independently of each other at speeds up to 25 μm s^{-1}. Therefore it was possible to switch within about 1 s between well-defined spatial stimulation patterns on length scales of tens of micrometers. One second was enough time for the concentration distribution around a bead to reach steady state (Supplementary Note 4).

DISCUSSION

The length scale of the chemical concentration patterns that can be generated by our technique depends on various factors. On the lower end, it is determined by the size of the particles that are releasing the stimulus. On the upper end, it is determined by the size of the microscope field of view in which particles can be optically manipulated and also by the number of particles that can be trapped simultaneously. Here we used particles with radii of 1.5–4 μm. Holographic optical tweezers setups allow trapping of about 100 particles simultaneously. Packing particles close together (particles with a diameter larger than about 1 μm can be packed to contact) allows mimicking large sources of chemoattractant with multiple small beads. The possibility to vary the size of microsources allows investigation of the response of cells to stimuli that vary in their degree of localization. For example, it has been found that localized release of cytokines from microparticles can induce a response in T cells that is different from the response to exogenous addition of cytokines[24]. Therefore, OMMs could, for example, enable further investigation into how paracrine delivery of agents may impact immune system cell function.

In addition to using multiple beads to create flexible spatial stimulation, we applied flexible temporal stimulation patterns to a cell by dynamically changing the distance of one or more beads away from the cell. The maximal frequency of stimulation we can create by our current implementation of holographic optical tweezers is about 30 Hz, which can be transmitted over a range of about 10 μm. However, if necessary, much larger stimulation frequencies could be generated with devices such as acousto-optical deflectors that can be driven in the range of kHz and above. Over larger distances, the maximal frequency that can be transmitted decreases (Supplementary Note 4).

Finally, OMMs offer a high degree of chemical flexibility. The PLGA particles that we used here trap the encapsulated molecules physically during the particle fabrication process. This enables the encapsulation and controlled release of a large variety of molecules including proteins, small peptides, fluorescent dyes, oligonucleotides and small-molecule drugs[20,25]. In contrast, caged molecules require the chemical development of a caged version for each type of molecule. Furthermore, PLGA is a well-established material that has no adverse side effects on cellular viability[26,27]. However, PLGA microparticles had been designed for release over long periods of time with large numbers of particles. Further optimization, including the use of other materials such as colloidosomes[28] and mesoporous silica nanoparticles[29,30], could potentially increase the concentration of released molecules by two orders of magnitude (Supplementary Note 7).

The spatial, temporal and chemical flexibility of OMMs make them applicable to a broad range of research areas in cell and developmental biology, where it is of interest to stimulate single cells or developing organisms locally with specific molecules.

Methods

Methods and any associated references are available in the online version of the paper at http://www.nature.com/naturemethods/.

Supplementary Material

Refer to Web version on PubMed Central for supplementary material.

Acknowledgments

We thank S. Dandekar, A. Houk, A. Millius and S. Wilson for help with cell culturing and sample preparation, A. Schaefer for helpful discussions, and M. Elimelech and W. Mitch for use of equipment. This work was supported by a fellowship (BMBF-LPD 9901/8-162) from the German Academy of Sciences Leopoldina to H.K., a US National Institutes of Health grant (1U54-RR0222332) and US National Science Foundation grants (CBET-0619674 and DBI–0619674) to E.R.D., a US National Institutes of Health grant (RO1-GM084040) to O.D.W and a US National Science Foundation CAREER grant (CBET-0747577) to T.M.F.

References

1. Gurdon JB, Bourillot PY. Morphogen gradient interpretation. Nature 2001;413:797–803. [PubMed: 11677596]
2. Meinhardt H. Models of biological pattern formation: from elementary steps to the organization of embryonic axes. Curr. Top. Dev. Biol 2008;81:1–63. [PubMed: 18023723]
3. Wadhams GH, Armitage JP. Making sense of it all: bacterial chemotaxis. Nat. Rev. Mol. Cell Biol 2004;5:1024–1037. [PubMed: 15573139]
4. Kay RR, Langridge P, Traynor D, Hoeller O. Changing directions in the study of chemotaxis. Nat. Rev. Mol. Cell Biol 2008;9:455–463. [PubMed: 18500256]
5. Van Haastert PJM, Devreotes PN. Chemotaxis: signalling the way forward. Nat. Rev. Mol. Cell Biol 2004;5:626–634. [PubMed: 15366706]
6. Cyster JG. Chemokines and cell migration in secondary lymphoid organs. Science 1999;286:2098–2102. [PubMed: 10617422]
7. Weiner OD. Regulation of cell polarity during eukaryotic chemotaxis: the chemotactic compass. Curr. Opin. Cell Biol 2002;14:196–202. [PubMed: 11891119]
8. Parent CA, Devreotes PN. A cell's sense of direction. Science 1999;284:765–770. [PubMed: 10221901]
9. Iglesias PA, Levchenko A. Modeling the cell's guidance system. Sci. STKE 2002;2002:re12. [PubMed: 12209053]
10. Skupsky R, Losert W, Nossal RJ. Distinguishing modes of eukaryotic gradient sensing. Biophys. J 2005;89:2806–2823. [PubMed: 16085764]
11. Herzmark P, et al. Bound attractant at the leading vs. the trailing edge determines chemotactic prowess. Proc. Natl. Acad. Sci. USA 2007;104:13349–13354. [PubMed: 17684096]
12. Beta C, Wyatt D, Rappel WJ, Bodenschatz E. Flow photolysis for spatiotemporal stimulation of single cells. Anal. Chem 2007;79:3940–3944. [PubMed: 17432827]
13. Samadani A, Mettetal J, van Oudenaarden A. Cellular asymmetry and individuality in directional sensing. Proc. Natl. Acad. Sci. USA 2006;103:11549–11554. [PubMed: 16864788]
14. Sun BY, Chiu DT. Synthesis, loading, and application of individual nanocapsules for probing single-cell signaling. Langmuir 2004;20:4614–4620. [PubMed: 15969173]
15. Dufresne ER, Grier DG. Optical tweezer arrays and optical substrates created with diffractive optics. Rev. Sci. Instrum 1998;69:1974–1977.
16. Dufresne ER, Spalding GC, Dearing MT, Sheets SA, Grier DG. Computer-generated holographic optical tweezer arrays. Rev. Sci. Instrum 2001;72:1810–1816.
17. Mejean CO, Schaefer AW, Millman EA, Forscher P, Dufresne ER. Multiplexed force measurements on live cells with holographic optical tweezers. Opt. Express 2009;17:6209–6217. [PubMed: 19365444]

18. Cooper JA. Effects of cytochalasin and phalloidin on actin. J. Cell Biol 1987;105:1473–1478. [PubMed: 3312229]
19. Urbanik E, Ware BR. Actin filament capping and cleaving activity of cytochalasin-B, cytochalasin-D, cytochalasin-E and cytochalasin-H. Arch. Biochem. Biophys 1989;269:181–187. [PubMed: 2916838]
20. Fahmy TM, Samstein RM, Harness CC, Saltzman WM. Surface modification of biodegradable polyesters with fatty acid conjugates for improved drug targeting. Biomaterials 2005;26:5727–5736. [PubMed: 15878378]
21. Servant G, et al. Polarization of chemoattractant receptor signaling during neutrophil chemotaxis. Science 2000;287:1037–1040. [PubMed: 10669415]
22. Zigmond SH. Ability of polymorphonuclear leukocytes to orient in gradients of chemotactic factors. J. Cell Biol 1977;75:606–616. [PubMed: 264125]
23. Ebert S, Travis K, Lincoln B, Guck J. Fluorescence ratio thermometry in a microfluidic dual-beam laser trap. Opt. Express 2007;15:15493–15499. [PubMed: 19550834]
24. Steenblock ER, Fahmy TM. A comprehensive platform for *ex vivo* T-cell expansion based on biodegradable polymeric artificial antigen-presenting cells. Mol. Ther 2008;16:765–772. [PubMed: 18334990]
25. Vasir JK, Labhasetwar V. Biodegradable nanoparticles for cytosolic delivery of therapeutics. Adv. Drug Deliv. Rev 2007;59:718–728. [PubMed: 17683826]
26. Cohen S, Yoshioka T, Lucarelli M, Hwang LH, Langer R. Controlled delivery systems for proteins based on poly(lactic/glycolic acid) microspheres. Pharm. Res 1991;8:713–720. [PubMed: 2062800]
27. Jiang WL, Gupta RK, Deshpande MC, Schwendeman SP. Biodegradable poly(lactic-co-glycolic acid) microparticles for injectable delivery of vaccine antigens. Adv. Drug Deliv. Rev 2005;57:391–410. [PubMed: 15560948]
28. Dinsmore AD, et al. Colloidosomes: selectively permeable capsules composed of colloidal particles. Science 2002;298:1006–1009. [PubMed: 12411700]
29. Slowing II, Trewyn BG, Giri S, Lin VSY. Mesoporous silica nanoparticles for drug delivery and biosensing applications. Adv. Funct. Mater 2007;17:1225–1236.
30. Carroll NJ, et al. Droplet-based microfluidics for emulsion and solvent evaporation synthesis of monodisperse mesoporous silica microspheres. Langmuir 2008;24:658–661. [PubMed: 18171093]

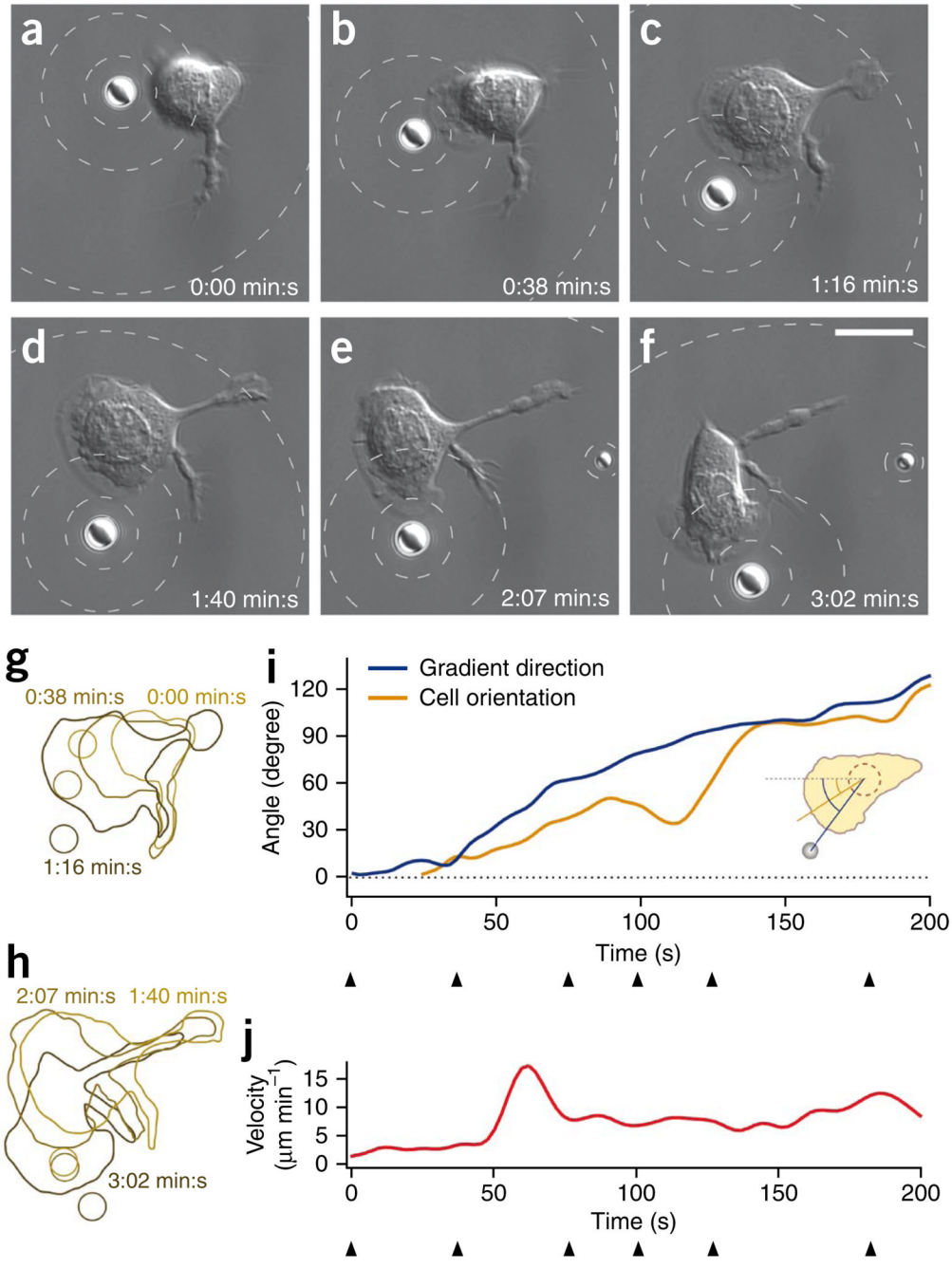

Figure 1.

A single optically manipulated bead loaded with chemoattractant induces directed polarization and migration of a neutrophil. (**a**–**f**) Differential interference contrast (DIC) microscopy images. PLGA particle loaded with fMLP was moved close to the membrane of an HL-60 cell (**a**). Cell polarized and migrated in the direction of the particle (**b**). Particle was moved counter-clockwise around the cell and the cell changed polarization and migration direction (**c**–**f**). The dashed contour lines indicate the spatially varying concentration of fMLP around the bead. The concentration on the surface of the bead (c_0) was 2 nM above the background, c_b = 20 nM. The contour lines show fMLP concentration levels of 50%, 25% and 10% of c_0 above c_b. Scale bars, 10 μm. (**g**,**h**) Sketches showing the cell contour and the bead contour from the images in

a–**f** (split into two sketches for clarity). The different colors of the contours indicate the different time points of the image series. (**i**,**j**) Direction of the gradient and cell orientation (direction from the center of the cell to the center of the leading edge) (**i**) and cell velocity (**j**) as a function of time. The directions were quantified as angles with respect to the dashed reference line. Arrowheads mark the time points shown in **a**–**f**.

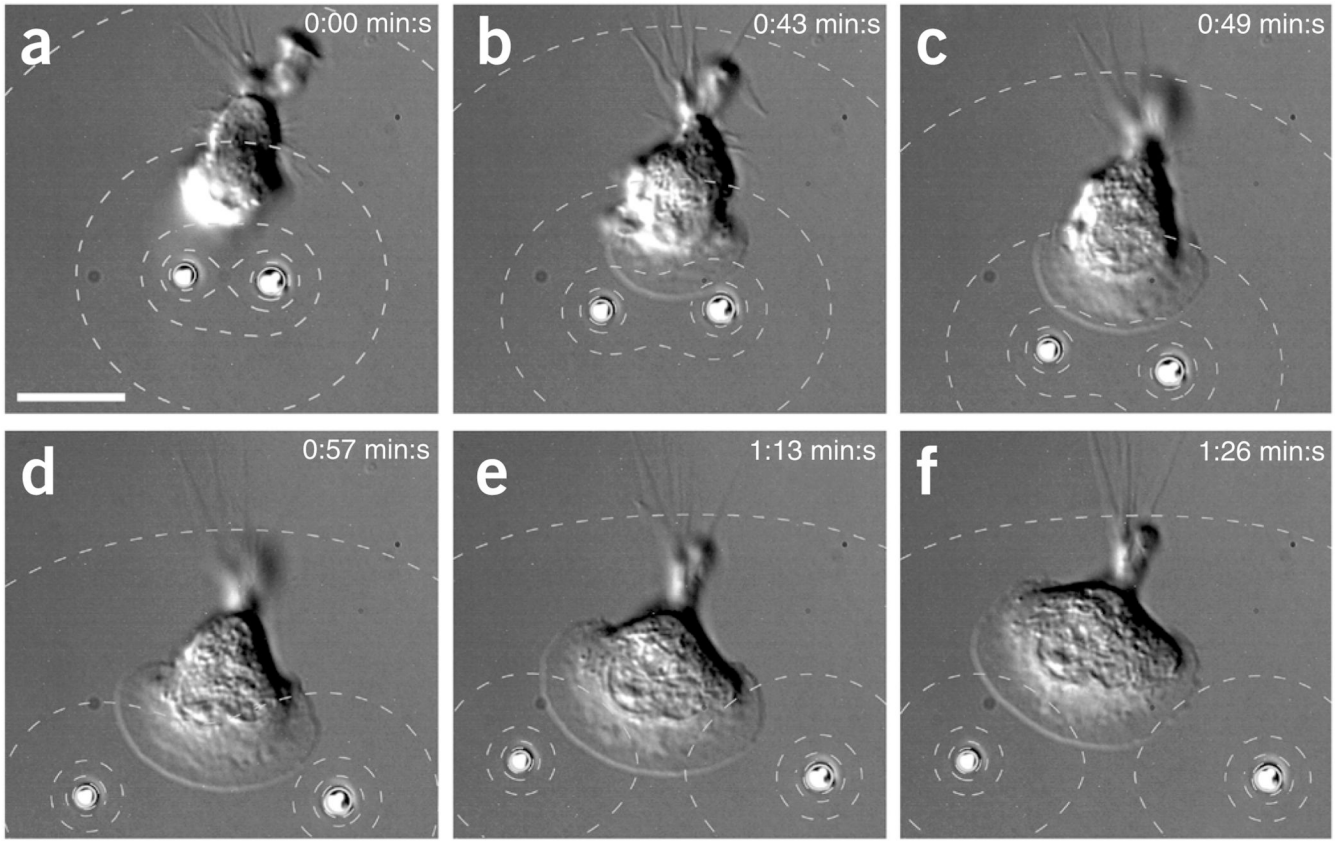

Figure 2.

Bipolar stimulation with chemoattractant induced formation and broadening of a lamellipodium. (**a**–**d**) Upon positioning of fMLP-loaded beads close to a HL-60 cell (**a**), the cell formed a lamellipodium in the direction of the beads (**b**) that broadened as the cell advanced toward the beads (**c**,**d**). (**e**,**f**) Ultimately, the lamellipodium reached its maximal size and the cell oriented toward the lower left bead. The contour lines in the DIC images show fMLP concentration (80, 60, 40, 20 and 10% of c_0 = 1 nM above the background c_b = 10 nM). Scale bars, 10 μm.

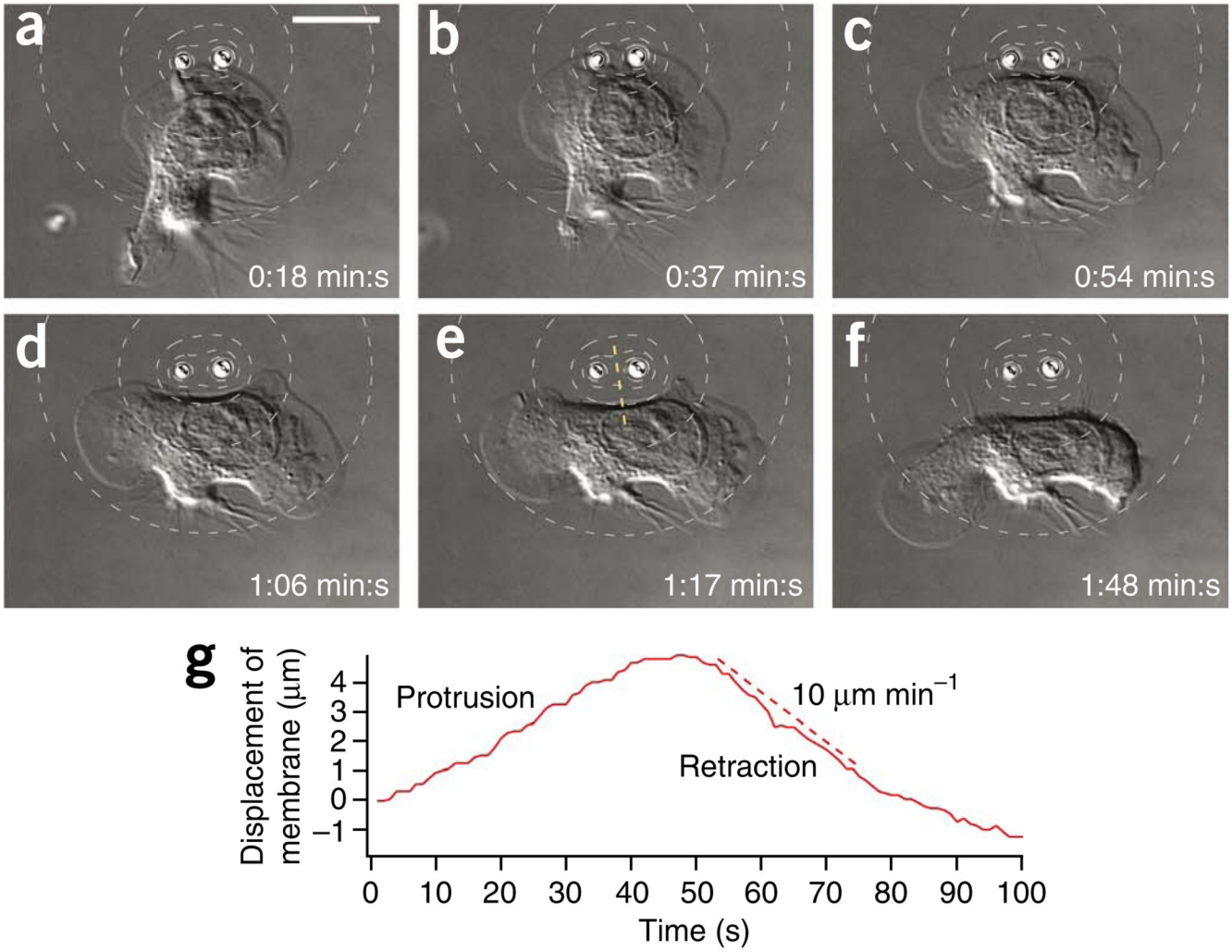

Figure 3.

OMMs of cytochalasin D induced highly localized retraction in the center of a lamellipodium. (**a**,**b**) Two beads releasing cytochalasin D close to the center of the lamellipodium of a migrating HL-60 cell. (**c**–**e**) Lamellipodium retracted in a small region around the beads (**c**) yielding a lamellipodium that was split into two parts (**d**,**e**). (**f**) Only one lamellipodium remained. The contour lines in the DIC images show cytochalasin D concentration (80, 60, 40, 20 and 10% of c_0 above the background). Scale bars, 10 μm. (**g**) The displacement of the membrane along the dashed yellow line in **e**.

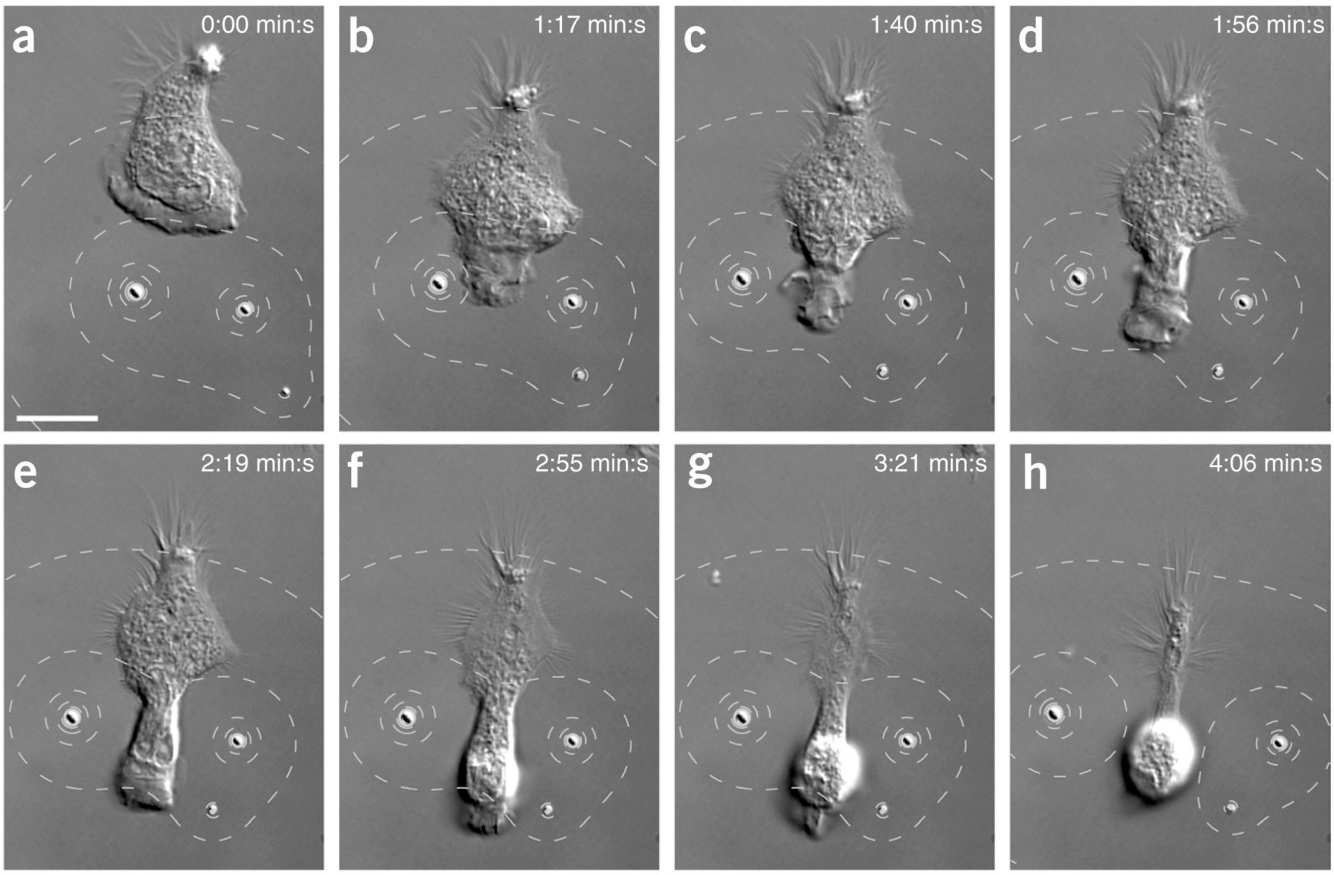

Figure 4.

Migrating cell squeezes between two optically manipulated microsources of cytochalasin D. (**a**) Two beads in front of a migrating HL-60 cell. (**b**–**f**) As the bead-to-bead distance increased to about 20 μm, the lamellipodium of the cell migrating toward the two particles retracted on the two sides closest to the beads while the central part of the leading edge continues to extend. (**g**,**h**) The cell rounded up and retracted its leading edge. The contour lines in the DIC images show cytochalasin D concentration (80, 60, 40, 20 and 10% of c_0 above background). Scale bars, 10 μm.

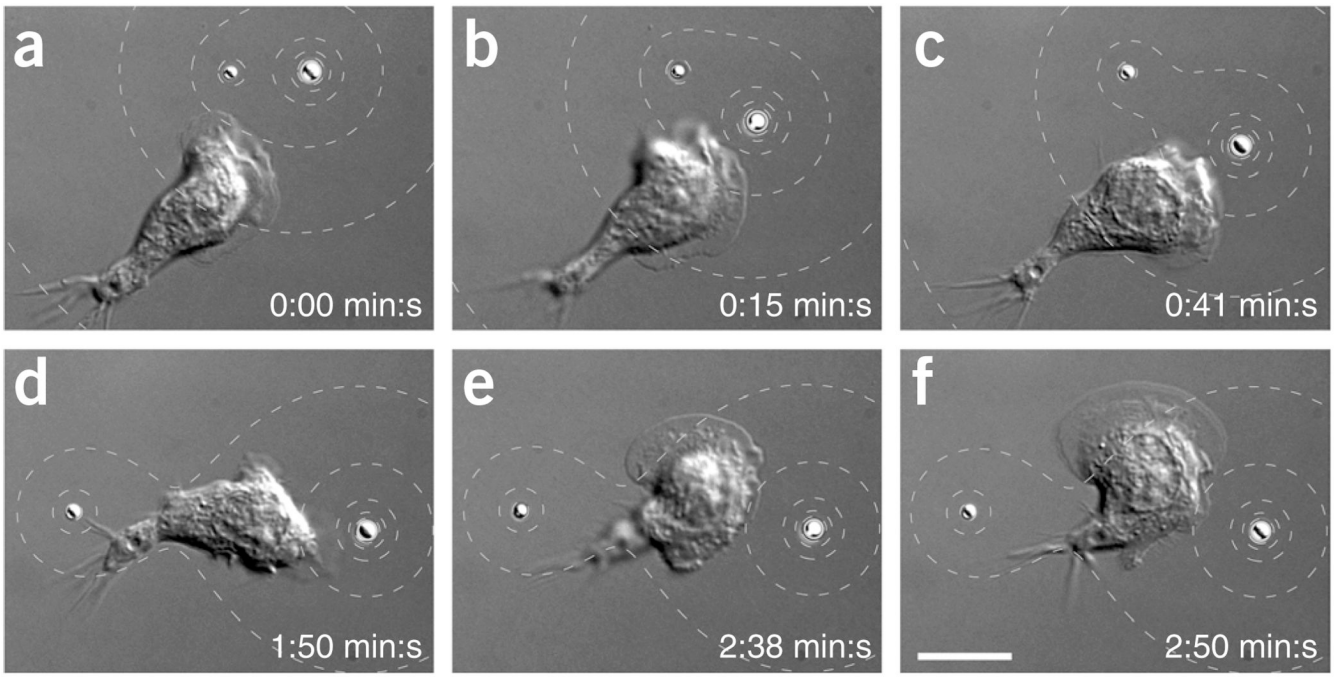

Figure 5.

Response of HL-60 cells to time-varying bipolar stimulus of cytochalasin D. (**a**–**c**) The cell stopped its migration and retracted its lamellipodium in response to two microsources of cytochalasin D placed in the direction of cell migration. (**d**) The two beads positioned on two opposing ends of the cell in the direction of cell polarization. (**e**,**f**) The cell repolarized in a direction perpendicular to the axis defined by the beads. The contour lines in the DIC images show cytochalasin D concentration (80, 60, 40, 20 and 10% of c_0 above background) Scale bars, 10 μm.